Study of Void Formation at the Lithium|Solid Electrolyte Interface

Pallab Barai[1], Till Fuchs[2], Enrico Trevisanello[2], Felix H. Richter[2],

Jürgen Janek[2] and Venkat Srinivasan[1*]

[1]Argonne National Laboratory, Lemont, IL, USA 60439

[2]Institute of Physical Chemistry and Center for Materials Research, Justus Liebig University Giessen, Heinrich-Buff-Ring 17, 35392, Giessen, Germany

Revised version for re-submission in

Chemistry of Materials

January 2024

[*]Corresponding author: Venkat Srinivasan (email: vsrinivasan@anl.gov)

Abstract

There is growing recognition of the critical role of void formation in lithium metal anodes in solid-state batteries and its impact on electrochemical performance. While experimental studies have demonstrated the challenges ensuing from void formation at the lithium metal interface with the solid electrolyte, there is a need to understand and quantify the role of intrinsic transport properties in lithium metal and impact of external stimuli, such as temperature, pressure, and current density. We develop this understanding by constructing a phase field based model that captures the evolution of void domains at the lithium|solid electrolyte interface. Growth of pores is driven by the fast removal of lithium from the interface during stripping at high current densities. Relative magnitudes of the bulk and surface lithium diffusivities, along with the applied current density, dictate the final pore morphology. Increasing the temperature results in faster diffusion while external applied pressure causes creep flow of lithium; both of which helps to mitigate the evolution of voids by quickly transporting metal from the bulk to the interface. Finally, a phase map as a function of temperature and pressure is developed as a guide to determine the regions that can lead to stable cycling of lithium metal.

Introduction

The lithium metal anode (LMA) has long been the most desired negative electrode for lithium ion batteries due to its extremely low potential (0 V vs. Li^+/Li) and high specific capacity (q_{th} ~ 3875 mAh/g).[1] However, lithium metal is highly reactive, which leads to significant reaction with most electrolytes and forms thick inhomogeneous solid-electrolyte-interphase (SEI) layers. Simultaneously, lithium deposition during the charging process is mostly nonuniform, and formation of dendrites over multiple cycles can lead to electronic shorting of cells.[2] This electrochemical instability of cycling lithium ions with liquid electrolytes has been a major bottleneck preventing widespread commercialization of lithium metal anodes. It has been argued that solid electrolytes, with the ability to generate a mechanical stress field around non-uniformly deposited lithium metal, can help to stabilize the deposition of lithium.[3] Unfortunately, further electrochemical studies on stiff garnet- (LLZO, Young's modulus ~ 150 GPa) and soft sulfide- (LPS, Young's modulus ~ 20 GPa) type solid electrolytes also clearly demonstrate the formation of lithium dendrites, and eventual shorting of cells over multiple cycles.[4, 5] Several arguments have been proposed to explain the mechanism of lithium dendrite growth in solid electrolytes, which includes the current focusing at the lithium|solid electrolyte interface due to either irregular contact, or non-uniformities in ion transport and electrochemical reactions.[6-16] All these arguments explain the propensity of lithium dendrite formation and propagation during the deposition process. However, none of them attempt to investigate the impact of the cycling, which involves alternating plating and stripping processes, on the overall dendrite formation.

It has been argued that during anodization, i.e., during lithium stripping, voids form at the lithium|solid electrolyte interface.[10, 17, 18] Formation of such porous region during discharge at the lithium|solid electrolyte interface limits the electrochemically active surface area. As a result, during the subsequent charging (meaning lithium plating) step, current focusing occurs, which can lead to dendrites. Deciphering the influence of void formation on current focusing and dendrite growth observed at the time of plating is crucial to understand how cycling can influence the lithium dendrite growth phenomena.[19]

Excessive formation of voids during the stripping process can fully delaminate the lithium metal electrode from the solid electrolyte, which can eventually lead to very high area specific resistance and complete cell failure.[18, 20] Formation of these pores at the time of lithium stripping depends on two types of factors, some are experimental variables, and the others are material specific properties, which can be listed as follows:[21]

i. Applied current density
ii. Externally applied pressure
iii. Temperature of operation
iv. Diffusion coefficient of lithium in the bulk of lithium metal
v. Surface energy between lithium metal and solid electrolyte

The dependencies of void formation on these parameters/properties have been determined based mostly on experimental evidence and atomistic calculations.[22, 23] Note that, microstructural (surface impurities, grain/grain-boundary microstructure) and morphological (surface roughness) features of lithium metal can also influence the void formation process.[24-26]

There exist a few detailed continuum level computational scheme that attempts to capture the formation and evolution of interfacial voids.[27] Some continuum modeling efforts attempted to elucidate the influence of external pressure in suppressing the interfacial voids.[14, 26] Others investigated the impact of pore size on the propensity of initiating void growth at the lithium|solid electrolyte interface.[28, 29] Detailed analysis based on atomistic (Density Functional Theory

(DFT), Molecular Dynamics (MD)) simulations have also been conducted to elucidate the nucleation of voids in the nanometer length scale, but the propagation and formation of micron sized pores was not captured successfully.[23, 25, 30, 31]

In the present context, a phase field based computational methodology is developed that can capture the evolution of pores at the lithium|solid electrolyte interface. It is hypothesized that surface diffusion plays a major role in the void formation process.[32-35] After the nucleation of a particular pore, in the absence of surface diffusion only a few atomic layers of lithium can dissolve before the entire electrode gets completely detached from the electrolyte.[23, 30] Experimentally observed interfacial voids reveal micrometer deep pore morphologies, which cannot be explained without a surface diffusion process.[18] The surface diffusion coefficient of lithium is assumed to be higher than the bulk diffusion coefficient of lithium, which helps to carry lithium ions from the bulk to the lithium|solid electrolyte interface in the vicinity of an evolving pore. Please note that the pits observed in lithium metal anodes during stripping with liquid electrolytes are not the same as the voids appearing at the lithium|solid electrolyte interface.[36] This difference arises because the lithium metal electrode, with or without pits, always remains in contact with the liquid electrolyte; whereas a void within a lithium anode adjacent to a solid electrolyte is electrochemically inactive.

Due to the relatively high homologous temperature of lithium metal at room temperature, externally applied pressure can cause substantial creep deformation.[37] Pressure induced creep flow of lithium metal can help minimize the extent of void formation during the stripping process.[20, 21] The operation temperature influences both the bulk and surface diffusivities of lithium metal, and it will have an impact on the void formation process. In this paper, firstly the void growth mechanism is discussed in detail. Next, the combined impact of external pressure and temperature of operation on the overall interfacial delamination is investigated. Finally, strategies to suppress the formation of pores during lithium stripping are discussed.

Methodology

In the present context a mesoscale level computational framework is developed that is capable of capturing the formation of micron sized pores at the lithium|solid electrolyte interface. LLZO based solid electrolytes are considered due to their inherent stability against lithium metal.[38] To provide some insight regarding pore depth, detailed experiments have been conducted with high quality imaging to extract the morphology of the interfacial voids. These experimental data help in the model fitting as well as in validation. Details of the experimental procedure and the computational framework adopted to generate the voids at the lithium|solid electrolyte interface are described below.

Experimental procedure to extract cross sectional micrographs: To generate a lithium metal electrode with pores at the surface, a symmetric Li|LLZO:Al|Li cell was built according to the procedure described by Krauskopf et al.[18, 21] leading to negligible interfacial resistances. Smoothness of the initial lithium metal electrodes was demonstrated in earlier publications through top view SEM images and also shown in Figure S1 (obtained using the FIB-SEM).[18, 39] One lithium electrode was then stripped unidirectionally with 100 μA cm^{-2} until a cut-off potential of 0.1 V was reached, as an indication of severe pore formation and morphological changes at the interface (voltage vs. time response shown in Figure S2 in SI). This electrode was then peeled off the garnet and analyzed with cryogenic focused-ion-beam scanning-electron-microscopy (FIB-SEM). These measurements were performed with a XEIA3 GMU SEM/Plasma-FIB (Tescan) in combination with a Leica VCT500 transfer module and a liquid nitrogen cooling stage (-130 °C).

Due to the complete electrochemical detachment of the lithium electrode from the solid electrolyte, the peeling off process did not introduce significant deformations within the lithium metal.[39] Before cooling and cutting into the lithium metal, a small platinum bar was deposited onto the material as a means to avoid artefacts at the very top of the sample, impeding the morphological analysis.

Computational Methodology: To capture the evolution of micrometer-sized pores at the lithium|solid electrolyte interface, a phase field based computational methodology is developed here. A particular conserved phase parameter ($\tilde{c}_{\mathrm{Li}}$) is introduced to model the evolution of the void phase within the lithium metal, where $\tilde{c}_{\mathrm{Li}} = 1$ indicates lithium metal and $\tilde{c}_{\mathrm{Li}} = 0$ denotes the pore domain.[40] The interphase region where the phase parameter changes from 0 to 1 indicates the surface of the lithium metal where the surface diffusion mechanism is activated. Charge transfer within lithium metal is assumed to occur through the flow of electrons (see Eq. (E1)), where the effective electronic conductivity of the computational domain $\left(\sigma_{\mathrm{Li,eff}}\right)$ is estimated as a function of the electronic conductivity of the lithium metal (σ_{Li}), void domain, and the local value of the phase parameter (see Eq. (E5)).[41] A constant current inflow boundary condition is applied at the current collector side of the lithium metal, and a reaction current density described by a Butler-Volmer characteristics is assigned to the solid electrolyte side (see Eqs. (E2) and (E3)). Detailed expression of the Butler-Volmer reaction kinetics is as follows:[3]

$$i_{\mathrm{BV}} = i_{0,\mathrm{ref}} \exp(\Delta\mu_{\mathrm{e}^-}/2RT) \cdot [\exp(F\eta_{\mathrm{s}}/2RT) - \exp(-F\eta_{\mathrm{s}}/2RT)] \quad (1)$$

Here, $i_{0,\mathrm{ref}}$ is the reference exchange current density, F indicates Faraday constant, R denotes the universal gas constant, T is temperature, $\Delta\mu_{\mathrm{e}^-}$ is the stress-induced electrochemical potential term, and η_{s} is the surface overpotential that is defined as, $\eta_{\mathrm{s}} = \phi_{\mathrm{s}} - \phi_{\mathrm{e}} - U_{\mathrm{Li}} + (\Delta\mu_{\mathrm{e}^-}/F)$, where ϕ_{s} is the potential in lithium electrode (which is equivalent to ϕ in Eq. (E1) in Table I), ϕ_{e} is the potential in the electrolyte (here, it is assumed that $\phi_{\mathrm{e}} = 0$), and U_{Li} indicates the open circuit potential for lithium deposition (in general, $U_{\mathrm{Li}} \sim 0.0\ V$).

Due to the conserved nature of the phase parameter, a Cahn-Hilliard type equation is solved to capture its evolution (see Eq. (E6) – (E8)). A boundary flux term, between lithium and solid electrolyte, associated with the Butler-Volmer reaction current, is introduced to capture the evolution of the void phase (see Eq. (E10)). The effective diffusivity of lithium atoms $\left(D_{\mathrm{Li,eff}}\right)$ within the metal electrode is defined as a combination of the volumetric (D_{v}) and surface (D_{s}) diffusivities (see Eq. (E12)).[41] Finally, the set of equations that govern the mechanical deformation of the lithium metal electrode under externally applied pressure is provided as Eqs. (E14) – (E22). Strain rate dependent viscoplastic deformation of the metal is considered along with a linear hardening law.[42, 43] All these equations, while solved together, provide the computational framework for capturing the evolution of micron sized pores at the lithium|solid electrolyte interface during the stripping process.

The computational domain where this set of equations is solved is provided in Figure 1(c). The lithium metal electrode is shown at the bottom, whereas the solid electrolyte is on top. The current collector is located below the metal electrode where inflow of current occurs, and the Butler-Volmer reaction current density is applied at the lithium|solid electrolyte interface. Note that capturing void formation is the focus of the present study, which predominantly exist within the lithium metal. Accordingly, no charge transport or mechanical equilibrium equations are solved within the solid electrolyte domain. The solid electrolyte is also assumed to experience minimal deformation under the externally applied pressure, and effectively acts as a rigid support. All the governing equations capturing the electronic conduction, lithium phase evolution, and external mechanical pressure induced creep are solved only within the lithium metal domain. To capture the evolution of the porous domain, a small void with a radius of 200 nm is assumed to exist initially at the lithium|solid electrolyte interface. During lithium stripping under sufficiently large magnitudes of externally applied current, predicting the growth of this small void region is the focus of the present research. Note that nucleation of the nanometer sized pores is not being investigated here. However, presence of heterogeneities within the electrolyte domain, for example, regions with enhanced ionic conductivity, can lead to the nucleation of voids within the lithium metal electrode.

Since the growth of only one void is simulated in the present context, estimating the exact size of the computational domain is very important. From a computational standpoint, as the interfacial void spans across the computational lithium metal domain, the electrode and electrolyte regions detach. As a result, the cell potential shoots up indicating a cell failure due to electrode detachment from the electrolyte and loss of electrochemically active surface area. Experimentally observed SEM and cross sectional micrographs shown in Figures 1(a) and 1(b) reveals that the interfacial voids are approximately 5 – 10 µm wide and 1 – 2 µm deep (zoomed in image of the pores shown in Figures S3).[18] Accordingly, a computational domain of size 10 µm x 6 µm is adopted for the computational analysis, which is depicted in Figure 1(c). The void nucleus is assumed to exist at the center, which grows and forms a micrometer sized pore during lithium stripping under externally applied anodic current densities.

Table I. List of equations solved for capturing the evolution of interfacial voids at the lithium|solid electrolyte interface.

Description of the equation	Mathematical expression	Equation number	Ref.
Governing equation for potential distribution	$\vec{\nabla} \cdot \left(\sigma_{\mathrm{Li,eff}} \vec{\nabla} \phi\right) = 0$	(E1)	[3, 40, 44]
Potential boundary condition on the current collector side	$\left(-\sigma_{\mathrm{Li,eff}} \vec{\nabla} \phi\right)\Big\|_{\substack{\text{Current}\\\text{Collector}}} = I_{\mathrm{app}}$	(E2)	

Potential boundary condition on the electrolyte side	$\left(-\sigma_{\mathrm{Li,eff}}\vec{\nabla}\phi\right)\big\vert_{\mathrm{Electrolyte}} = i_{\mathrm{BV}}$	(E3)	
Zero current boundary condition on the left and right boundary	$\left(-\sigma_{\mathrm{Li,eff}}\vec{\nabla}\phi\right)\big\vert_{\substack{\text{Left and Right}\\ \text{Boundary}}} = 0$	(E4)	
Conductivity within the lithium metal phase	$\sigma_{\mathrm{Li,eff}} = \sigma_{\mathrm{Li}}\tilde{c}_{\mathrm{Li}}$	(E5)	
Evolution equation for the lithium metal phase	$\dfrac{\partial \tilde{c}_{\mathrm{Li}}}{\partial t} = \vec{\nabla}\cdot\left(D_{\mathrm{Li}}\vec{\nabla}\mu_{\mathrm{Li}} - \tilde{c}_{\mathrm{Li}}v_{\mathrm{Li}}\right)$	(E6)	
Chemical potential for lithium	$\mu_{\mathrm{Li}} = \delta F_{\mathrm{Li}}/\delta\tilde{c}_{\mathrm{Li}}$	(E7)	
The total energy functional for lithium metal	$F_{\mathrm{Li}} = \displaystyle\int \left[\begin{array}{l} A_{\mathrm{Li}}\tilde{c}_{\mathrm{Li}}^{2}(1-\tilde{c}_{\mathrm{Li}})^{2} \\ +\dfrac{1}{2}\beta_{\mathrm{Li}}\left\vert\vec{\nabla}\tilde{c}_{\mathrm{Li}}\right\vert^{2}\end{array}\right] dv$	(E8)	
Lithium flux boundary condition on the current collector side	$\left(-D_{\mathrm{Li}}\vec{\nabla}\mu_{\mathrm{Li}}\right)\big\vert_{\substack{\text{Current}\\ \text{Collector}}} = 0$	(E9)	[40, 41]
Lithium flux boundary condition on the electrolyte side	$\left(-D_{\mathrm{Li}}\vec{\nabla}\mu_{\mathrm{Li}}\right)\big\vert_{\mathrm{Electrolyte}} = \max\left(0, \dfrac{i_{\mathrm{BV}} - I_{\mathrm{app}}}{F}\right)$	(E10)	
Zero lithium flux boundaries on the left and right side	$\left(-D_{\mathrm{Li}}\vec{\nabla}\mu_{\mathrm{Li}}\right)\big\vert_{\substack{\text{Left and Right}\\ \text{Boundary}}} = 0$	(E11)	
Effective lithium diffusivity within the lithium metal electrode	$D_{\mathrm{Li}} = h(\tilde{c}_{\mathrm{Li}})\cdot D_{\mathrm{v}} + h'(\tilde{c}_{\mathrm{Li}})\cdot D_{\mathrm{s}}$ here, $h(\tilde{c}_{\mathrm{Li}}) = \tilde{c}_{\mathrm{Li}}^{3}(10 - 15\tilde{c}_{\mathrm{Li}} + 6\tilde{c}_{\mathrm{Li}}^{2})$	(E12)	
Equilibrium equation for mechanical stress	$\vec{\nabla}\cdot\boldsymbol{\sigma} = 0$	(E13)	
Constitutive relation between stress and strain tensors	$\boldsymbol{\sigma} = \boldsymbol{C}_{\mathbf{Li,eff}}^{\mathbf{el}}:\boldsymbol{\epsilon}^{\mathbf{el}}$ here, $\boldsymbol{C}_{\mathbf{Li,eff}}^{\mathbf{el}} = \boldsymbol{C}_{\mathbf{Li,eff}}^{\mathbf{el}}\left(YM_{\mathrm{Li,eff}}, \nu_{\mathrm{Li,eff}}\right)$	(E14)	
Effective Young's modulus and Poisson's ratio as a function of lithium concentration	$YM_{\mathrm{Li,eff}}, \nu_{\mathrm{Li,eff}} = \tilde{c}_{\mathrm{Li}}\cdot(YM_{\mathrm{Li}}, \nu_{\mathrm{Li}})$	(E15)	
Additive decomposition of total strain tensor	$\boldsymbol{\epsilon}^{\mathbf{tot}} = \boldsymbol{\epsilon}^{\mathbf{el}} + \boldsymbol{\epsilon}^{\mathbf{vp}}$	(E16)	
Viscoplastic strain rate as a function of deviatoric stress tensor	$\dot{\boldsymbol{\epsilon}}^{\mathbf{vp}} = \dot{\gamma}\cdot(3\boldsymbol{s}/2q_{\mathrm{vm}})$	(E17)	[42, 43]
Multiplying factor as a function of the von Mises stress	$\dot{\gamma} = \left(q_{\mathrm{vm}} - \sigma_{\mathrm{y}}\right)/G_{\mathrm{vp}}$	(E18)	
Von Mises stress as a function of the deviatoric stress tensor	$q_{\mathrm{vm}} = \sqrt{\dfrac{3}{2}\boldsymbol{s}:\boldsymbol{s}}$	(E19)	
Equivalent viscoplastic strain rate as a function of viscoplastic strain rate tensor	$\dot{\epsilon}_{\mathrm{eq}}^{\mathrm{vp}} = \sqrt{\dfrac{2}{3}\dot{\boldsymbol{\epsilon}}^{\mathbf{vp}}:\dot{\boldsymbol{\epsilon}}^{\mathbf{vp}}}$	(E20)	

Yield stress as a function of the equivalent viscoplastic strain	$\sigma_{\mathrm{y}} = \sigma_{\mathrm{y,0}} + H\epsilon_{\mathrm{eq}}^{\mathrm{vp}}$	(E21)	

Table II. List of parameters used for running the simulations is provided below.

Name	Symbol	Unit	Value	Reference
Conductivity of lithium	σ_{Li}	$\mathrm{S/m}$	$1.1\mathrm{x}10^{7}$	[40]
Exchange current density	i_0	$\mathrm{A/m^2}$	100	[45, 46]
Faraday constant	F	$\mathrm{C/mol}$	96485	--
Universal gas constant	R	$\mathrm{J/(mol - K)}$	8.314	--
Temperature	T	$^{\circ}\mathrm{C}$	25	[18, 21]
Volumetric diffusivity of lithium	D_{v}	$\mathrm{m^2/s}$	10^{-15}	[47]
Surface diffusivity of lithium	D_{s}	$\mathrm{m^2/s}$	2×10^{-12}	[33, 34, 48]
Surface energy of lithium	γ_{Li}	$\mathrm{J/m^2}$	0.5	[40, 48]
Interfacial width	l_{Li}	µm	0.5	Assumed
Young's modulus of lithium	YM_{Li}	GPa	10	[3]
Poisson's ratio of lithium	ν_{Li}	--	0.42	[3]
Yield strength of lithium	$\sigma_{\mathrm{y,0}}$	MPa	0.7	[37]
Hardening modulus of lithium	H	MPa	2.0	[49]
Viscosity of lithium	G_{vp}	GPa	0.5	Assumed

Results and Discussion

Providing a mechanistic understanding behind the formation of micron sized voids at the lithium|solid-electrolyte interface during the stripping process is the focus of the present study.[18, 20, 23, 30] To elucidate the propagation of these interfacial pores, it is important to extract some information regarding their morphology, such as, width, depth, etc. Accordingly, scanning electron microscopy (SEM) imaging of the surface of a stripped lithium electrode (electrochemical stripping of lithium was continued till the voltage signal exceeded the upper cutoff) is conducted to estimate the width of the porous domains, which is shown in Figure 1(a). It is evident that the width of the porous domains ranges approximately between 5 µm to 15 µm, with an average width of 10 µm.[18] Focused ion beam scanning electron microscopy (FIB-SEM) imaging of the cross section of a Li|LLZO interface is conducted according to the technique described in the Methodology section, and the final porous microstructures are depicted in Figure 1(b), also highlighted by the red lines. Depth of the pores varies approximately between 1 μm to 2 μm (please note the difference in scale bar in Figures 1(a) and 1(b)).[18, 21] Cross sectional FIB-SEM images of the lithium surface, previously in contact to the electrolyte, is shown in Figure S3 (within SI) at different resolutions for better visualization of the interfacial void domains. The void domains demonstrated in Figures 1(a) and 1(b) at the lithium|solid electrolyte interface are obtained by stripping lithium under a current density of 0.1 mA/cm^2. Impact of these interfacial voids on the voltage and overall cell performance will also be elucidated.[18, 20, 21, 45] The manuscript is divided into the following subsections:

i) Understanding the mechanism of void formation and impact of surface diffusion.

ii) Comparison with experimental results.

iii) Impact of initial pore size on lithium|solid electrolyte interfacial detachment.

iv) Influence of externally applied pressure.

v) Effect of increasing self-diffusivity of lithium within the bulk

vi) Stability map between applied pressure and temperature.

All the above-mentioned aspects will be analyzed using the phase field based mesoscale level computational scheme described in the Methodology section and schematically demonstrated in Figure 1(c). Note that in this analysis the ceramic electrolyte is assumed to be completely rigid and free from any defects and imperfections. All the charge mass and force balance relations are solved within the lithium metal electrode.

Understanding the mechanism of void formation and impact of surface diffusion: In order to understand the mechanism behind the interfacial void formation process, growth of a pore at the lithium|solid electrolyte interface, as predicted by the phase field based computational model, is shown in Figure 2. The main plot in Figure 2 demonstrates the voltage response with time during stripping induced growth of an interfacial pore at an applied current density of 0.1 mA/cm^2 and negligible external pressure (a zoomed in version of the voltage vs. time curve is provided in Figure S4 within the SI section). Starting from an initial pore nucleus, changes to the pore morphology with stripping is shown in the surrounding figures marked A to E within Figure 2. The yellow region indicates a void domain, whereas dark blue denotes lithium metal. Distribution of reaction current at the lithium|solid electrolyte interface containing an interfacial pore is shown in Figure S5 within the supplementary information (SI) section, which clearly indicates significant focusing of reaction current at the edges of the porous domains. Note that a constant value of the self-diffusivity of lithium within the bulk is assumed, and the surface diffusion coefficient is 2000 times larger than the self-diffusion coefficient.[34, 47, 48] Such high magnitude of the surface diffusion coefficient is only achievable for pristine lithium surfaces. If lithium oxide or lithium carbonate form on the void surfaces due to side reactions, the magnitude of surface diffusivity may become much smaller, even less than the bulk diffusivity of lithium.[23] Formation of a pristine interface between lithium and void regions is assumed in the remaining portion of the manuscript.

During stripping, lithium is extracted from the top of the domain, which, in an ideal case, should be completely compensated by diffusion of lithium from the bulk to the interface. However, due to the limited self-diffusivity of lithium, all the required lithium cannot come from the bulk. Since the surface diffusion mechanism is faster than the self-diffusion process, some lithium is carried through the surface of the pore from the bulk to the interface. This removal of lithium metal from the bulk causes the pores to penetrate deep into the metal anode. The voltage responses for each of the pore morphologies are denoted in the voltage vs. time curve of Figure 2 by the green circles and also marked A to E. Note that the applied current density is always estimated based on the pristine surface area. It is evident that unless the void region spans the entire lithium|solid electrolyte interface, the voltage drop is almost negligible.[18, 50] This can be attributed to the extremely large conductivity of lithium metal and very high exchange current density between lithium and LLZO, which effectively minimizes the potential drop across the computational domain.[18, 21, 40, 45] Only when the pore spans across the lithium|solid electrolyte interface and the electrolyte completely loses contact with the metal electrode, the voltage starts to rise indefinitely (see a zoomed in image of the voltage vs. time curve in Figure S4(b) in SI).[18, 21] The amount of time required to completely detach the metal electrode from the LLZO electrolyte depends on the surface diffusion coefficient and pore morphology, which will be discussed next. Note that current constriction at the lithium|solid electrolyte interface is taken into consideration in the developed model. However, due to the extremely high exchange current density at the lithium|solid electrolyte interface, and very small width of the computational domain (only ~ 10 μm), the current constriction induced increase in cell voltage is negligible, and not evident in the voltage vs. time response shown in Figure 2.

The pore morphology, or its depth, depends on the magnitude of the surface diffusion coefficient. To elucidate this aspect, the evolution of two different void domains are demonstrated in Figures 3(a) and 3(b) obtained under two different magnitudes of surface diffusion coefficients, which are 500 and 5000 times larger than their bulk counterpart, respectively.[33, 34, 48] It is evident from Figure 3(a) that smaller surface diffusivity leads to shallow pores, whereas Figure 3(b) indicates that a larger surface diffusion coefficient leads to deeper void domains. Metals with larger surface diffusivity can easily deliver more material from the bulk and quickly transport it to the interface where the electrochemical reaction occurs. As a result, higher surface diffusion coefficients lead to deeper pores. On the contrary, lack of strong surface diffusion prevents the void domain from going deep into the bulk and confines it close to the surface.[23, 30]

Corresponding voltage vs. time curves as obtained with different magnitudes of surface diffusivities are depicted in Figure 3(c). It is evident for both the surface diffusion coefficients that unless the void domain completely spans across the entire lithium|solid electrolyte interface, the potential drop is negligible.[18, 21] After complete detachment and loss of electrochemically active surface area, the overpotential increases indefinitely.[21, 45] From the time required for the overpotential to increase rapidly, it is possible to estimate the time needed for complete interfacial detachment between the lithium metal and LLZO.[21] It is possible to conclude from Figure 3(c) that smaller surface diffusivity leads to quicker interfacial detachment, and larger surface diffusion delays the complete loss of electrochemically active surface area. This observation is consistent with the evolution of pore morphology, where higher surface diffusivity carries more lithium from the bulk to the interface and delays the overall interfacial detachment. Note that a constant magnitude of applied current density (0.1 mA/cm^2) is assumed in these simulations, and no external pressure is exerted on the lithium metal electrode. During stripping and plating of lithium, higher magnitudes of surface diffusivity are always beneficial, because it can sustain enhanced contact area between the electrode and the electrolyte. Despite formation of the deeper pores under large surface diffusivity, the enhancement in electrochemically active surface area leads to a decrease in current focusing during the subsequent plating processes.

It has already been demonstrated that the pore morphology at the lithium|solid electrolyte interface is dictated by the surface diffusion coefficient. The external driving force that leads to the formation of interfacial porous domains is provided by the applied current density.[20, 29, 30, 45] Depending on the rate at which lithium is stripped at the interface, lithium metal needs to be delivered from the bulk through the self-diffusion (or bulk diffusion) and surface diffusion processes.[18, 21] Operation at higher current density results in faster removal of lithium from the interface and metal atoms need to be transferred quickly from the bulk. Incomplete delivery of lithium from the bulk to the interface results in growth of the void space, which can eventually lead to complete interfacial detachment. This clearly alludes to a competition between the rate of lithium removal (or applied current density) and rate at which lithium arrives from the bulk to the interface (or the surface diffusion coefficient).

Accordingly, a phase map between surface diffusivity and applied current is proposed in Figure 4 where the green/turquoise domain indicates no interfacial delamination, and the yellow region denotes complete detachment. Lithium stripping simulations are continued for 4 hours for generating this phase map. Data points that demonstrated 100% contact after the 4 hour long stripping are characterized as "stable interface" (green/turquoise region), whereas even partial detachment, or contact fraction less than 100% after 4 hours led to the conclusion of "delaminated interface" (shown in yellow in Figure 4). It is evident that increasing the applied current density rapidly removes lithium from the interface, leading to growth of the interfacial void domains. In contrast, increasing the surface diffusivity helps to carry more lithium from the bulk to the interface and slows down void growth and detachment. For surface diffusivity ratios in the range of 1 to 10^3 $(1 < (D_\mathrm{s}/D_\mathrm{v}) < 10^3)$, the surface diffusion mechanism is not strong enough to completely suppress the formation of voids. Mostly, the removal of porous domains occurs through the bulk diffusion process for these smaller magnitudes of surface diffusivity $\left((D_\mathrm{s}/D_\mathrm{v}) < 10^3\right)$, which renders a stability map independent of the surface diffusivity (denoted by the vertical green/turquois domain in Figure 4). However, for higher magnitudes of surface diffusion coefficient $\left((D_\mathrm{s}/D_\mathrm{v}) > 10^3\right)$, the surface diffusivity mechanism is capable of completely suppressing the interfacial void formation (indicated by the inclined stability limit). Note that no external pressure was applied while generating the phase map, and the bulk (or volumetric or self) diffusivity is maintained constant (as provided in Table II). The combined influence of surface diffusion and current density on the overall void formation mechanism has not been reported so far. Our analysis helps to elucidate the stripping-induced lithium|solid electrolyte interfacial detachment mechanism.

Comparison with experimental results: Several studies attempted to understand the evolution of interfacial voids as a function of applied current density through experimental means.[17, 18, 20-22, 45] Quicker interfacial detachment was reported under higher stripping current densities.[20, 21] To understand the influence of applied current on the morphology of the interfacial void domains, the evolution of pores at the lithium|solid electrolyte interface is investigated under different current densities using computational means. The computationally predicted pore morphologies for stripping current densities of 0.05 mA/cm^2, 0.1 mA/cm^2 and 0.2 mA/cm^2 are shown in Figures 5(a), 5(b) and 5(c), respectively. It is evident that increasing the applied current results in shallow pores. This can be attributed to the faster removal of lithium from the interface under higher current densities. Also, during operation under large currents, limited transport of lithium from the bulk to the interface causes the void domains to remain confined near the electrochemically active surface instead of going deep. On the other hand, Figure 5(a) shows that deep pores form at lower current densities, where a substantial amount of lithium metal can diffuse from the bulk to the reactive interface causing the porous domains to penetrate deep inside the electrode. The corresponding variation in voltage with respect to time is shown in Figure 5(d). It is evident that the voltage response increases rapidly only after complete detachment of the metal electrode from the solid electrolyte. The time required for the void domain to completely span the entire electrode is characterized as the "time to cell failure", which can be easily extracted from the time needed for the voltage signal to increase (as shown in Figure 5(d)).

The computationally predicted "time to cell failure" for the three different current densities of 0.05 mA/cm^2, 0.1 mA/cm^2 and 0.2 mA/cm^2 are compared with the experimental observations in Figure 5(e).[21] It is evident that adoption of a surface diffusion coefficient 2000 times larger than the bulk diffusion coefficient leads to a relatively good agreement with the experimental observations. Note that experimental results were adopted from the existing literature, which were conducted earlier by some of the authors.[18, 21, 45]

Another important aspect regarding the pore morphology is the depth of the porous domains, which can be compared with the experimental observations. The cryogenic focused ion beam scanning electron microscopy (FIB-SEM) image of the Li interface (as shown in Figure 1(b)) clearly reveals that the void domains are approximately 1 – 2 μm in depth. Note that all these images are extracted after stripping lithium at 0.1 mA/cm^2. Altering the stripping current density should lead to some variation in the pore depth because the pore morphology depends on how fast lithium ions are removed from the interface.[21, 45] The computationally predicted depths of pores are plotted in Figure 5(f) and compared with the experimental observations. Only one experimental data point exists because visualization of the pore size and shape is conducted under only one stripping current density, which is 0.1 mA/cm^2. Relatively good agreement between the computational predictions and experimental observations helps to further validate the developed computational scheme.

Impact of initial pore size on lithium|solid electrolyte interfacial detachment: Several computational studies have pointed out that interfacial pores of any size cannot grow and delaminate the metal electrode from the ceramic solid electrolyte.[28, 30] The existing models suggest that only pores larger than a certain critical size can generate enough tensile stress that can detach the electrode form the electrolyte.[28, 29] In the present study, the existence of a critical pore size is investigated from a mass transport standpoint, and its correlation with the applied current density is elucidated. If there exists a small void at the lithium|solid electrolyte interface, two different scenarios are possible during lithium stripping, depending on the stripping current density and the magnitude of the surface and bulk diffusion coefficients:

a) If the pore is very small in size (in the range of a few nanometers), the bulk metal is located very close to the interface. Metal atoms needs to diffuse only over a small distance, and can easily diffuse via self-diffusion without the need of the faster surface diffusion. The small void usually gets dissolved within such a scenario, where mass transport limitations are not encountered.

b) On the other hand, for relatively large interfacial voids, the bulk metal is far away from the electrochemically active interface. Hence, lithium from the bulk needs to diffuse a longer distance to reach the interface, which is not possible only via self-diffusion. The faster surface diffusion needs to be invoked, which stabilizes the void domains and eventually causes their growth in size.[18]

The maximum size of pores that can completely dissolve under a certain stripping current density is characterized as the "critical pore size". Pores larger than this critical size cannot dissolve and tend to grow with time. The critical pore size is plotted in Figure 6 as a function of the applied current density for lithium metal anodes without external pressure. A fixed magnitude of the self-diffusion coefficient of lithium is used, whereas the surface diffusion coefficient is assumed to be 2000 times larger than the self-diffusion coefficient. It is evident that with increasing stripping current, more lithium atoms from the bulk need to be transported to the interface faster. Hence, at higher currents, even the smaller pores become unstable because of their participation in carrying atoms from the bulk to the interface through the surface diffusion mechanism. The results presented in Figure 6 show that under realistic applied current densities (~ 1 mA/cm^2), even very small interfacial voids with size in the range of tens of nanometers can grow and delaminate the electrode from the electrolyte.[17, 20-22] In other words, any formation of pores – almost regardless of their size – has to be avoided, as otherwise they grow and degrade the interface.

Influence of externally applied pressure: It has been argued using both experimental and computational means that application of compressive external pressure mitigates the interfacial detachment between the lithium metal electrode from the ceramic solid electrolyte.[18, 20-23, 29, 30] Creep flow of lithium from the bulk to the interface is expected to delay the growth of the void domains, and remove or reduce the size of the interfacial voids under sufficiently large external pressure.[18, 29, 30] This unique influence of mechanical stress induced creep flow of lithium metal on the interfacial void growth mechanism is captured using the developed phase field based mesoscale computational framework by implementing the force equilibrium equations along with the mass balance relations. Lithium metal is assumed to deform following a viscoplastic mechanism, and the plastic flow initiates after the local stress level exceeds the yield limit.[37] The existing literature is unclear about the exact yield limit of lithium metal, offering a range of measured values from as low as 0.7 MPa to 15 MPa.[14, 37] However, existing experimental reports indicate that stripping-induced evolution of void space can be substantially mitigated by the application of compressive external pressure of magnitude around 7.5 MPa.[21, 51] Adoption of lithium yield strength in the range of 15 MPa cannot successfully capture creep-induced removal of interfacial voids at 7.5 MPa pressure. Hence, in the present context, lithium yield strength of about 0.7 MPa is assumed to properly model the impact of creep flow in the evolution of porous domains.

Simulations are conducted to understand the growth of the interfacial voids under 0.2 mA/cm^2, and various externally applied pressures ranging between 0 MPa to 15 MPa.[21] The voltage vs. time curves shown in Figure 7 indicate that for compressive stresses ranging between 0 MPa to 4 MPa, the porous domain grows and completely delaminates the lithium anode from the ceramic solid electrolyte, which results in a sudden increase in the voltage response. Increasing the external pressure delays the growth of the interfacial pores, which is evident from the fact that under 0 MPa complete delamination occurs in less than 2 hours, whereas it takes more than 2 hours to completely delaminate the electrode from the electrolyte at higher pressures (such as, 4 MPa). Note that even after complete delamination, the lithium electrode can carry some stress due to the presence of the diffuse interface between solid lithium and void domain, and prevents the computational domain from experiencing infinitely large stresses. Interestingly, under pressures around 6 MPa the interfacial void neither completely spans across the computational domain, nor is the interfacial pore entirely removed even after running the simulation for 10 hours. As a result, the voltage vs. time curve never shoots up. Finally, for pressures of 8 MPa and higher, the interfacial void gets completely eliminated due to creep flow of metal from the bulk to the interface. Time evolution of the interfacial void domain under 8 MPa pressure and 0.2 mA/cm^2 applied current density is depicted in Figure S6 within the SI section. Hence, it can be concluded that under an applied current density of 0.2 mA/cm^2, the critical pressure needed to suppress the interfacial void domains is around 8 MPa, which is clearly demonstrated in Figure 7. It is interesting to note that even under pressures higher than the critical value (8 MPa for an applied current of 0.2 mA/cm^2), the interfacial voids grow in size initially, but eventually, with time, get completely suppressed due to the creep flow of lithium metal. This increase and decrease in void size can be attributed to the time taken by the creep deformation mechanism to reach its steady state value.[37] During this transient time range, the formation and growth of the interfacial voids can still occur. However, once the creep deformation reaches its steady state magnitude, suppression of the void domain becomes evident. If the magnitude of external pressure increases, the complete suppression of voids occurs earlier, which can be concluded from the fact that it requires around 8 hours to remove the voids under 8 MPa pressure, whereas under a pressure of 15 MPa, a pore-free interface can be obtained within 4 hours. This is consistent with the fact that under larger magnitudes of external pressure, creep flow becomes faster. The non-steady voltage response in cells cycled under higher magnitudes of external pressures, such as 6 – 15 MPa, can be attributed to the change in electrochemically active surface area due to increase and decrease in void size under external pressure, as well as the effect of mechanical stress on the electrochemical reaction (see Eq. (1)). Also, the increase in voltage response with increasing external pressure can be attributed to the stress-potential coupling terms in the Butler-Volmer reaction current expression shown in Eq. (1). Note that some earlier experimental studies on the electrochemical stripping of a silver metal electrode under external pressure indicated the formation, and subsequent removal, of interfacial pores in a periodic fashion, which led to oscillation in voltage response over time.[52-54] The developed computational model is not capable of capturing such oscillatory behavior in its present form, but can possibly help to delineate the interplay between surface diffusion and creep deformation in stripping of metal electrodes.

It is clearly pointed out in Figure 7 that a critical pressure of 8 MPa is needed for complete removal of the interfacial pores under an applied current density of 0.2 mA/cm^2. The variation in critical pressure as a function of the applied current is worth investigating next. Accordingly, several simulations were run at various applied currents ranging between 0.05 – 2 mA/cm^2 to estimate the magnitude of critical pressure needed to completely suppress the interfacial voids.[20, 21] The results are plotted in Figure 8 where the applied current densities are shown along the *x*-axis and the magnitude of the critical pressure is shown along the *y*-axis, both in log scales. It is evident that increasing the applied current results in a similar increase in the magnitude of the critical pressure. It can be explained from the fact that under higher currents, the rate of lithium removal from the lithium|solid electrolyte interface is very high, and faster creep flow of lithium metal is needed, under higher pressure, for maintaining complete contact between the two surfaces. The data points in Figure 8 can be roughly connected by a straight line, which follows the power law type relation $P_{\text{crit}} \sim I_{\text{app}}^{n}$, where P_{crit} is the critical pressure under a particular applied current density denoted by I_{app}. The exponent n has a value of 1.1 for this particular case, where the surface diffusion coefficient is assumed to be 2000 times larger than the self-diffusivity of lithium and the lithium yield strength is assumed to be constant at 0.7 MPa.[33, 37, 47, 48] Changing the surface diffusion coefficient and/or yield limit of the metal can result in a different value of the exponent. This analysis indicates that under realistic applied currents of 1 mA/cm^2, pressures around 50 – 60 MPa need to be applied for maintaining a stable interface between the lithium metal electrode and the LLZO solid electrolyte. Note that the computationally predicted critical pressure needed to keep the lithium|solid electrolyte interface in contact far exceeds the experimentally observed values, which can possibly be attributed to the variations in elastic-plastic properties of the solid electrolyte and the lithium metal electrode.[20, 51] Figure 8 also acts as a phase map, where the data points lying above and below the blue line can help battery engineers estimate the desired external pressures needed to stabilize the lithium stripping process. Following experimental efforts, a separate approach can also be adopted to estimate critical pressures needed to keep the lithium metal electrode in contact with the solid electrolyte, where the magnitude of external pressure is decreased in steps while one of the electrode continuously strips lithium under a constant applied current density.[51] The simulated voltage vs. time curves for three different applied current densities of 0.1, 0.3 and 0.5 mA/cm^2 are shown in Figure S7 within the supplementary information (SI) section, which appears to qualitatively correlate with the experimental observations.[51] The critical pressures obtained from Figure S7 may not correlate with the critical pressures reported in Figure 8 because of the 5 hour stripping time limit adopted in Figure S7, which may be insufficient to completely detach the lithium electrode from the solid electrolyte.

Effect of increasing self-diffusivity of lithium within the bulk: In the present study, the self-diffusivity of lithium is kept constant at an experimentally observed value.[47] Self-diffusion determines how fast lithium atoms move within the bulk metal. However, it is possible to influence self-diffusion coefficient of lithium in multiple ways, such as:

a) Increasing the temperature of operation[47]
b) Alloying lithium with other metals where faster diffusion of lithium is possible[21]

Hence, the influence of changing the magnitude of the bulk diffusion of lithium on the overall pore formation mechanism is worth investigating. Accordingly, several simulations are run under an applied current of 0.1 mA/cm^2 and zero external pressure, while varying the bulk diffusivity of lithium metal. The results are shown in Figure 9, where the time for failure and pore depth is denoted by the black circles and red triangles, respectively. From Figure 9 it is evident that lowering the bulk diffusion coefficient to half of its initial value results in shallow pores and complete detachment is achieved quickly. On the other hand, increasing the bulk diffusivity by a factor of two results in much deeper pores, which takes longer to span across the entire computational domain. All these observations are consistent with the physical understanding that altering the bulk diffusivity of lithium changes the speed of lithium metal atoms arriving from the bulk to the interface, and subsequently influences the pore morphology and the time required for lithium|solid electrolyte detachment induced cell failure. Lithium stripping induced growth of interfacial pores under bulk diffusivities four times (or more) larger than the initial value leads to stable electrochemical operation without any growth of the interfacial porous domains, which is denoted by the green region in Figure 9. Please note that the magnitude of the surface diffusion coefficient is assumed to be 2000 times larger than the bulk diffusivity.[33, 34, 48] Experimental results showed that alloying magnesium with lithium can substantially stabilize the lithium stripping process.[21] It is well known that the diffusion coefficient of lithium atoms within the Li-Mg alloy is around six times larger than the self-diffusivity of pure lithium.[21] Hence, stable electrochemical stripping of lithium at 0.1 mA/cm^2 while using magnesium as alloying element is justified by the present computational analysis. However, for stabilizing the lithium stripping process under more realistic reaction current densities of 1 mA/cm^2 will require much larger bulk diffusivity in lithium metal.

Stability map as function of applied pressure and temperature: A battery scientist/engineer usually has the capability to control the pressure that acts on the cell and the temperature of operation.[20, 22, 55] Earlier results presented as part of this study clearly indicate that increasing the compressive stress on the lithium|solid electrolyte interface can substantially enhance the creep flow of lithium metal and eventually mitigate the growth of interfacial pores.[20, 21, 29, 30] Similarly, with increasing temperature of operation, the bulk and surface diffusivity of lithium should increase, which is again expected to delay, or completely eliminate, the growth of interfacial voids. Accordingly, a phase map, as function of the applied pressure and temperature, is shown in Figure 10, indicating the operating conditions where stable stripping of lithium is expected (green domains), and where complete detachment between the electrode and electrolyte should occur (yellow region). The entire phase map is generated assuming a stripping current density of 1 mA/cm^2, and the surface diffusivity is assumed to be 2000 times larger than the bulk value.[33, 34, 47, 48] It is evident from the phase map as well as the basic physical understanding that increasing both the pressure and temperature results in stable stripping of lithium. Figure 10 reveals that cell cycling above 70 °C stabilizes the stripping process even without any external pressure. Similarly, at room temperature, around 50 – 60 MPa pressure needs to be applied for blocking the growth of interfacial voids. This phase map can provide practically relevant guidelines for battery engineers to estimate the operating conditions for successful operation of lithium metal anodes.

Conclusions

Evolution of void domains at the lithium|solid electrolyte interface is investigated in the present study using a phase field based computational framework. Importance of surface diffusivity on lithium pore walls in determining the morphology of the porous domains is clearly demonstrated. The developed methodology is capable of capturing pore morphologies that are a few microns deep and span over tens of micrometers. Evolution of the voids is dictated by the competition between how fast the lithium ions are removed from the electrochemically active interface and how quickly they are replenished by transport of atoms from the bulk.[18] If the stripping-induced removal of lithium ions is fast enough, the pores grow, which leads to early detachment between the lithium metal anode and the ceramic solid electrolyte. However, if the flow of lithium from the bulk to the interface dominates, the growth of porous domains slows down and the lithium|solid electrolyte delamination is delayed, or void formation is averted entirely. Note that the adhesive strength between the electrode and electrolyte has no impact on the void formation process because the evolution of interfacial voids does not occur by pulling the electrode surface apart from the electrolyte. The electrochemical dissolution of metal from the electrode leads to the formation of the interfacial voids, which can possibly be avoided by enhancing the flow of lithium from the bulk to the interface.

Transport of lithium from the bulk to the interface can be enhanced by two possible mechanisms:[18, 20-22, 47, 48]

a) Increasing the temperature of operation leads to faster bulk and surface diffusion,

b) Applying external compressive stress can result in creep flow of lithium metal.

Advantages associated with increasing the temperature of operation and cell cycling under external pressure in mitigating the interfacial voids are thoroughly investigated as part of this work. It is concluded from Figure 10 that stable stripping of lithium can be achieved at 70 °C without the application of any external pressure under a realistic current density of 1 mA/cm^2. Also, the minimum pressure required to stabilize the lithium stripping process follows a power law relation with the applied current.

During lithium stripping, whether a pore grows in size is dictated by its size as well as the applied current density. Formation of a conformal lithium electrode surface, with roughness in the range of nanometers, may prevent the formation of interfacial voids even under realistic stripping current densities of 1 – 10 mA/cm^2. Other strategies already investigated to mitigate the void formation are alloying lithium with other metals that can help to enhance the lithium bulk diffusion coefficient.[21] Once pore formation cannot be circumvented, "self-healing" by a contact-mediating liquid, for example, ionic liquids, may provide a solution.[56] Another strategy can be the implementation of intermediate rest intervals during the stripping process, which can possibly lead to higher stripping capacity through diffusion mediated healing of the interfacial void regions (see Figure S8 in the Supplementary Information section).[57]

Note that during realistic operation in a full cell, the lithium metal anodes are not stripped indefinitely.[58] Depending on the cathode capacity and rate of operation, cell discharge (stripping of lithium metal electrode) at an extremely high rate might occur for a very short period of time.[59] Also, due to the extremely high exchange current density between lithium metal anode and LLZO solid electrolyte, complete contact between the electrode and electrolyte domains may not be necessary for successful operation.[45] External pressures, or other contact mediating liquids, that are capable of terminating the “propagation” of interfacial pores, but not the entire porous domain, should be sufficient for continued stripping of the metal electrode. More detailed simulation of a larger computational domain with multiple interfacial voids are needed for estimating the exact magnitude of pressure, or amount of alloying metals, or volume of ionic liquids, necessary to complete the cell discharge process.

Supporting Information

Contains additional FIB-SEM images demonstrating the lithium surface before and after stripping, some experimentally observed and computationally predicted voltage vs. time curves, and evolution in pore morphology at lithium|solid electrolyte interface as predicted by model.

Acknowledgements

This work was supported by the Assistant Secretary for Energy Efficiency and Renewable Energy, Office of Vehicle Technologies of the U.S. Department of Energy under Contract No. DE-AC02-06CH11357 under the Advanced Battery Materials Research (BMR). Financial support within the

German-US program funded by DOE and BMBF (Federal Ministry for Education and Research) and the projects LISI and LISI-2 (project identifiers 3XP0224E and 3XP0509B is acknowledged (J.J. and T.F.).

References

1. Janek, J. and W.G. Zeier, *A solid future for battery development.* Nature Energy, 2016. **1**(9): p. 1-4.
2. Krauskopf, T., et al., *Physicochemical concepts of the lithium metal anode in solid-state batteries.* Chemical Reviews, 2020. **120**(15): p. 7745-7794.
3. Monroe, C. and J. Newman, *The impact of elastic deformation on deposition kinetics at lithium/polymer interfaces.* Journal of The Electrochemical Society, 2005. **152**(2): p. A396.
4. Dixit, M.B., et al., *Synchrotron imaging of pore formation in Li metal solid-state batteries aided by machine learning.* ACS Applied Energy Materials, 2020. **3**(10): p. 9534-9542.
5. Lewis, J.A., et al., *Linking void and interphase evolution to electrochemistry in solid-state batteries using operando X-ray tomography.* Nature Materials, 2021. **20**(4): p. 503-510.
6. Barai, P., et al., *Mechanical stress induced current focusing and fracture in grain boundaries.* Journal of The Electrochemical Society, 2019. **166**(10): p. A1752.
7. Barai, P., et al., *The role of local inhomogeneities on dendrite growth in LLZO-based solid electrolytes.* Journal of the Electrochemical Society, 2020. **167**(10): p. 100537.
8. Cheng, E.J., A. Sharafi, and J. Sakamoto, *Intergranular Li metal propagation through polycrystalline Li6. 25Al0. 25La3Zr2O12 ceramic electrolyte.* Electrochimica Acta, 2017. **223**: p. 85-91.
9. Cheng, L., et al., *Effect of surface microstructure on electrochemical performance of garnet solid electrolytes.* ACS applied materials & interfaces, 2015. **7**(3): p. 2073-2081.
10. Koshikawa, H., et al., *Dynamic changes in charge-transfer resistance at Li metal/Li7La3Zr2O12 interfaces during electrochemical Li dissolution/deposition cycles.* Journal of power sources, 2018. **376**: p. 147-151.
11. Porz, L., et al., *Mechanism of lithium metal penetration through inorganic solid electrolytes.* Advanced Energy Materials, 2017. **7**(20): p. 1701003.
12. Shen, F., et al., *Effect of pore connectivity on Li dendrite propagation within LLZO electrolytes observed with synchrotron X-ray tomography.* ACS Energy Letters, 2018. **3**(4): p. 1056-1061.
13. Tian, H.-K., B. Xu, and Y. Qi, *Computational study of lithium nucleation tendency in Li7La3Zr2O12 (LLZO) and rational design of interlayer materials to prevent lithium dendrites.* Journal of Power Sources, 2018. **392**: p. 79-86.
14. Zhang, X., et al., *Pressure-driven interface evolution in solid-state lithium metal batteries.* Cell Reports Physical Science, 2020. **1**(2): p. 100012.
15. Tian, H.-K., et al., *Interfacial electronic properties dictate Li dendrite growth in solid electrolytes.* Chemistry of Materials, 2019. **31**(18): p. 7351-7359.

16. Eckhardt, J.K., et al., *Interplay of Dynamic Constriction and Interface Morphology between Reversible Metal Anode and Solid Electrolyte in Solid State Batteries.* Acs Applied Materials & Interfaces, 2022. **14**(31): p. 35545-35554.
17. Jow, T. and C. Liang, *Interface Between Solid Electrode and Solid Electrolyte—A Study of the Li/LiI (Al2 O 3) Solid-Electrolyte System.* Journal of The Electrochemical Society, 1983. **130**(4): p. 737.
18. Krauskopf, T., et al., *Toward a fundamental understanding of the lithium metal anode in solid-state batteries—an electrochemo-mechanical study on the garnet-type solid electrolyte Li6. 25Al0. 25La3Zr2O12.* ACS applied materials & interfaces, 2019. **11**(15): p. 14463-14477.
19. Manalastas Jr, W., et al., *Mechanical failure of garnet electrolytes during Li electrodeposition observed by in-operando microscopy.* Journal of Power Sources, 2019. **412**: p. 287-293.
20. Kasemchainan, J., et al., *Critical stripping current leads to dendrite formation on plating in lithium anode solid electrolyte cells.* Nature materials, 2019. **18**(10): p. 1105-1111.
21. Krauskopf, T., et al., *Diffusion limitation of lithium metal and Li–Mg alloy anodes on LLZO type solid electrolytes as a function of temperature and pressure.* Advanced Energy Materials, 2019. **9**(44): p. 1902568.
22. Jow, T. and C. Liang, *Interface between solid anode and solid electrolyte-effect of pressure on Li/LiI (Al2O3) interface.* Solid State Ionics, 1983. **9**: p. 695-698.
23. Yang, M. and Y. Mo, *Interfacial Defect of Lithium Metal in Solid-State Batteries.* Angewandte Chemie, 2021. **133**(39): p. 21664-21671.
24. Shi, F.F., et al., *Lithium metal stripping beneath the solid electrolyte interphase.* Proceedings of the National Academy of Sciences of the United States of America, 2018. **115**(34): p. 8529-8534.
25. Venturi, V. and V. Viswanathan, *Thermodynamic Analysis of Initial Steps for Void Formation at Lithium/Solid Electrolyte Interphase Interfaces.* Acs Energy Letters, 2022. **7**(6): p. 1953-1959.
26. Yan, H.H., et al., *How Does the Creep Stress Regulate Void Formation at the Lithium-Solid Electrolyte Interface during Stripping?* Advanced Energy Materials, 2022. **12**(2).
27. Agier, J.A.B., et al., *Void growth within Li electrodes in solid electrolyte cells.* Acta Materialia, 2022. **240**.
28. Roy, U., N. Fleck, and V. Deshpande, *An assessment of a mechanism for void growth in Li anodes.* Extreme Mechanics Letters, 2021. **46**: p. 101307.
29. Shishvan, S.S., N.A. Fleck, and V.S. Deshpande, *The initiation of void growth during stripping of Li electrodes in solid electrolyte cells.* Journal of Power Sources, 2021. **488**: p. 229437.
30. Yang, M., et al., *Interfacial Atomistic Mechanisms of Lithium Metal Stripping and Plating in Solid-State Batteries.* Advanced Materials, 2021. **33**(11): p. 2008081.
31. Shishvan, S., et al., *Void growth in metal anodes in solid-state batteries: Recent progress and gaps in understanding.* European Journal of Mechanics-A/Solids, 2023: p. 104998.
32. Davidson, R., et al., *Formation of magnesium dendrites during electrodeposition.* ACS Energy Letters, 2018. **4**(2): p. 375-376.

33. Jäckle, M. and A. Groß, *Microscopic properties of lithium, sodium, and magnesium battery anode materials related to possible dendrite growth.* The Journal of chemical physics, 2014. **141**(17): p. 174710.
34. Jäckle, M., et al., *Self-diffusion barriers: possible descriptors for dendrite growth in batteries?* Energy & Environmental Science, 2018. **11**(12): p. 3400-3407.
35. Janek, J. and S. Majoni, *Influence of Mechanical Pressure on Ionic Charge Transport Across the Ag| AgI-Interface-Periodic Oscillations of Interfacial Properties.* Defect and Diffusion Forum, 1996. **129 - 130**: p. 243 - 252.
36. Wood, K.N., et al., *Dendrites and pits: Untangling the complex behavior of lithium metal anodes through operando video microscopy.* ACS central science, 2016. **2**(11): p. 790-801.
37. LePage, W.S., et al., *Lithium mechanics: roles of strain rate and temperature and implications for lithium metal batteries.* Journal of The Electrochemical Society, 2019. **166**(2): p. A89.
38. Kim, Y., et al., *Electrochemical stability of Li6. 5La3Zr1. 5M0. 5O12 (M= Nb or Ta) against metallic lithium.* Frontiers in Energy Research, 2016. **4**: p. 20.
39. Fuchs, T., et al., *Increasing the Pressure-Free Stripping Capacity of the Lithium Metal Anode in Solid-State-Batteries by Carbon Nanotubes.* Advanced Energy Materials, 2022. **12**(26).
40. Chen, L., et al., *Modulation of dendritic patterns during electrodeposition: A nonlinear phase-field model.* Journal of Power Sources, 2015. **300**: p. 376-385.
41. Wang, Y.U., *Computer modeling and simulation of solid-state sintering: A phase field approach.* Acta materialia, 2006. **54**(4): p. 953-961.
42. Dunne, F. and N. Petrinic, *Introduction to computational plasticity*. 2005, Oxford ; New York: Oxford University Press. xiv, 241 p.
43. Neto, E.A.d.S., D. Perić, and D.R.J. Owen, *Computational methods for plasticity : theory and applications*. 2008, Chichester, West Sussex, UK: Wiley. xix, 791 p.
44. Newman, J.S. and K.E. Thomas-Alyea, *Electrochemical systems*. 3rd ed. 2004, Hoboken, N.J.: J. Wiley. xx, 647 p.
45. Krauskopf, T., et al., *The fast charge transfer kinetics of the lithium metal anode on the garnet-type solid electrolyte Li6. 25Al0. 25La3Zr2O12.* Advanced Energy Materials, 2020. **10**(27): p. 2000945.
46. Sharafi, A., et al., *Surface chemistry mechanism of ultra-low interfacial resistance in the solid-state electrolyte Li7La3Zr2O12.* Chemistry of Materials, 2017. **29**(18): p. 7961-7968.
47. Dologlou, E., *Self-Diffusion in Solid Lithium.* Glass Physics and Chemistry, 2010. **36**(5): p. 570-574.
48. Gaissmaier, D., et al., *Microscopic Properties of Na and Li-A First Principle Study of Metal Battery Anode Materials.* Chemsuschem, 2020. **13**(4): p. 771-783.
49. Barai, P., K. Higa, and V. Srinivasan, *Lithium dendrite growth mechanisms in polymer electrolytes and prevention strategies.* Physical Chemistry Chemical Physics, 2017. **19**(31): p. 20493-20505.
50. Eckhardt, J.K., et al., *3D Impedance Modeling of Metal Anodes in Solid-State Batteries-Incompatibility of Pore Formation and Constriction Effect in Physical-Based 1D Circuit Models.* Acs Applied Materials & Interfaces, 2022. **14**(37): p. 42757-42769.

51. Wang, M.J., R. Choudhury, and J. Sakamoto, *Characterizing the Li-Solid-Electrolyte Interface Dynamics as a Function of Stack Pressure and Current Density.* Joule, 2019. **3**(9): p. 2165-2178.
52. Janek, J. and S. Majoni, *Investigation of Charge-Transport across the Ag-Vertical-Bar-Agi-Interface .1. Occurrence of Periodic Phenomena during Anodic-Dissolution of Silver.* Berichte Der Bunsen-Gesellschaft-Physical Chemistry Chemical Physics, 1995. **99**(1): p. 14-20.
53. Majoni, S. and J. Janek, *Periodic electrochemical oscillations at a solid-solid electrode.* Solid state ionics, 1996. **85**(1-4): p. 247-250.
54. Majoni, S. and J. Janek, *Investigation of charge transport across the Ag| AgI-interface:(II) Dilatometric study of the anodic dissolution of silver.* Berichte der Bunsengesellschaft für physikalische Chemie, 1998. **102**(5): p. 756-762.
55. Ren, D., et al., *Investigation of lithium plating-stripping process in Li-ion batteries at low temperature using an electrochemical model.* Journal of The Electrochemical Society, 2018. **165**(10): p. A2167.
56. Fuchs, T., et al., *Working Principle of an Ionic Liquid Interlayer During Pressureless Lithium Stripping on Li6. 25Al0. 25La3Zr2O12 (LLZO) Garnet-Type Solid Electrolyte.* Batteries & Supercaps, 2021. **4**(7): p. 1145-1155.
57. Lee, K. and J. Sakamoto, *Effect of Surface Nature on Stripping of in Situ Li Anodes and Enhancement of Its Stripping Capacity*, in *2023 ECS - The Electrochemical Society*. 2023, The Electrochemical Society. p. 974.
58. Albertus, P., et al., *Status and challenges in enabling the lithium metal electrode for high-energy and low-cost rechargeable batteries.* Nature Energy, 2018. **3**(1): p. 16-21.
59. Fredericks, W.L., et al., *Performance metrics required of next-generation batteries to electrify vertical takeoff and landing (VTOL) aircraft.* ACS Energy Letters, 2018. **3**(12): p. 2989-2994.

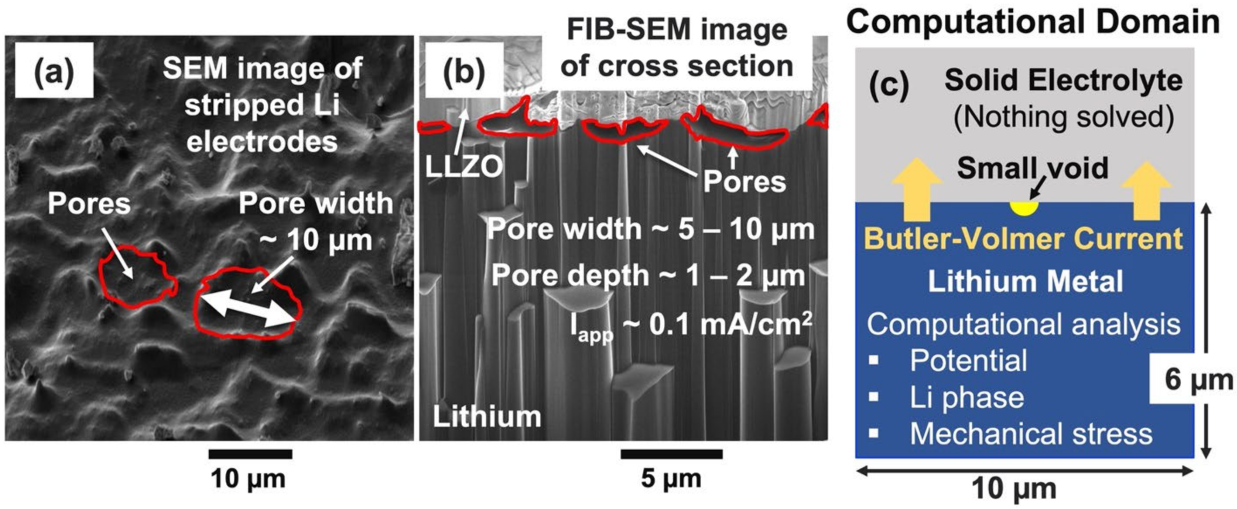

Figure 1. (a) Scanning electron microscopy (SEM) image of the surface of the stripped lithium metal. Presence of a very rough surface indicates the formation of pores during the electrochemical stripping process. (b) Focused ion beam (FIB) SEM image of the Li/LLZO cross section indicating that the depth of the interfacial pores is in the range of 1 µm – 2 µm. Lithium is located at the bottom and platinum is on top. Platinum is used for better visualization. From Figures 1(a) and 1(b) it is also evident that the width of the pores ranges between 5 µm – 10 µm. (c) Demonstration of the computational domain with the lithium metal electrode at the bottom (dark blue region) and solid electrolyte at the top (ash colored domain). Due to lithium stripping, a flow of lithium ions occurs from the lithium metal to the electrolyte. The solid electrolyte is assumed to be rigid, and the grain boundaries do not influence the reaction current at the lithium|solid electrolyte interface. Evolution of electrical potential, lithium phase and mechanical stresses are solved within the lithium metal electrode.

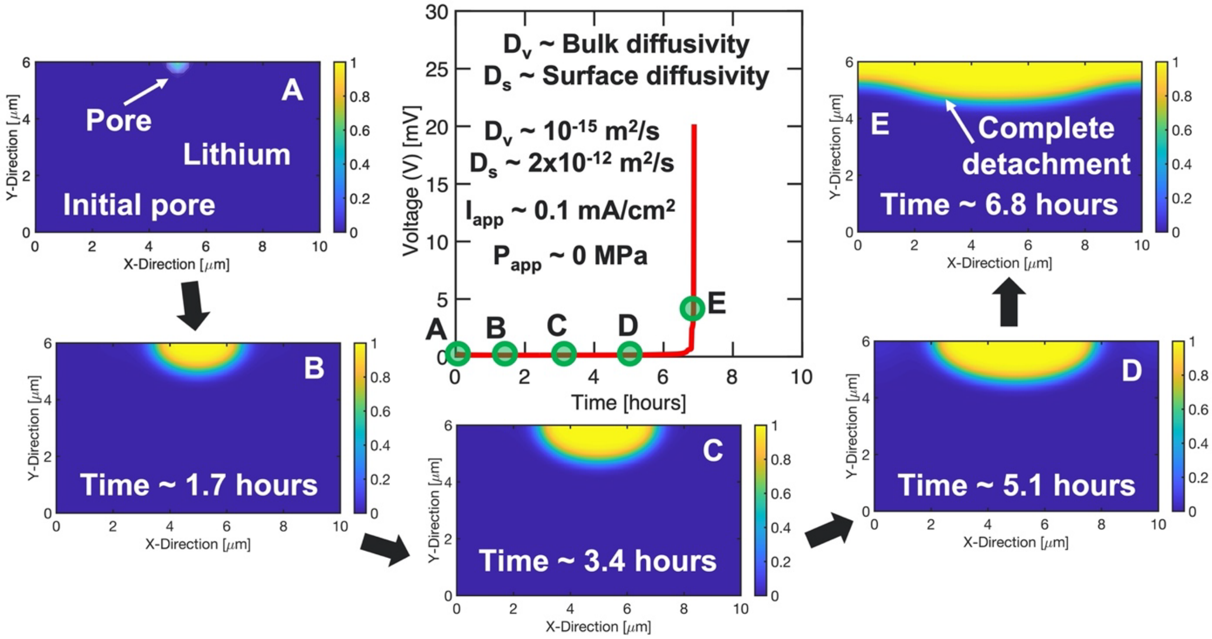

Figure 2. Pore evolution and corresponding increase in voltage with time. Change in voltage with time is shown in the main figure. The voltage remains small for a long time, and suddenly shoots up. This sudden increase in cell potential is associated with complete detachment between lithium and solid electrolyte. The corresponding pore morphologies are shown by the images marked A, B, C, D and E (yellow indicates pores and dark blue denotes lithium). Due to the very high exchange current density between lithium and LLZO, the overpotential is small as long as there remains some contact between the lithium and solid electrolyte. As soon as complete detachment between the electrode and electrolyte occurs, the cell potential shoots up. These computational predictions correlate with the experimental observations reported in the literature (see Krauskopf et al., *ACS AMI* 2019 11 14463 – 14477). The applied current density is maintained at 0.1 mA/cm^2 and no external pressure is applied. Surface diffusivity of lithium is assumed to be 2000 times larger than bulk diffusivity.

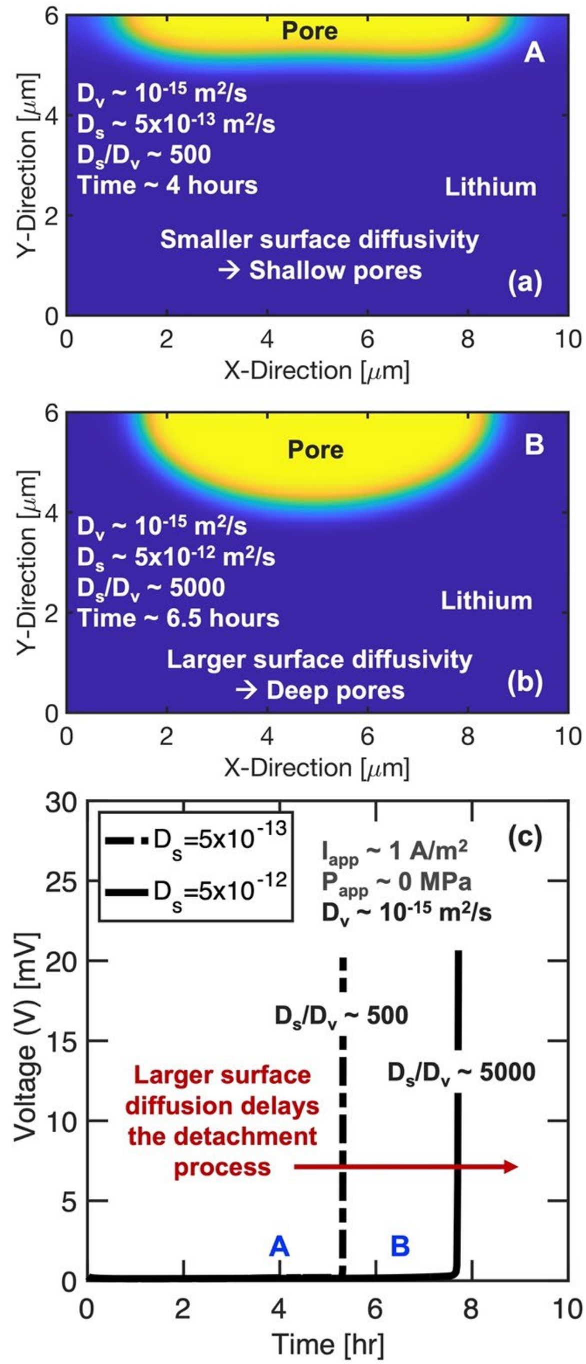

Figure 3. Influence of surface diffusivity on pore morphology and voltage profile. (a) Pore morphology with $D_s/D_v \sim 500$, applied current density of $0.1\ \mathrm{mA/cm^2}$ and zero applied pressure. (b) Pore morphology with $D_s/D_v \sim 5000$ under the same current and pressure as the previous case. It is evident that larger surface diffusivity leads to formation of deeper pores. (c) Evolution of voltage with time for the two different values of surface diffusivity. Smaller values of D_s causes shallow pores, which quickly spans across the electrode and results in early detachment of the interface.

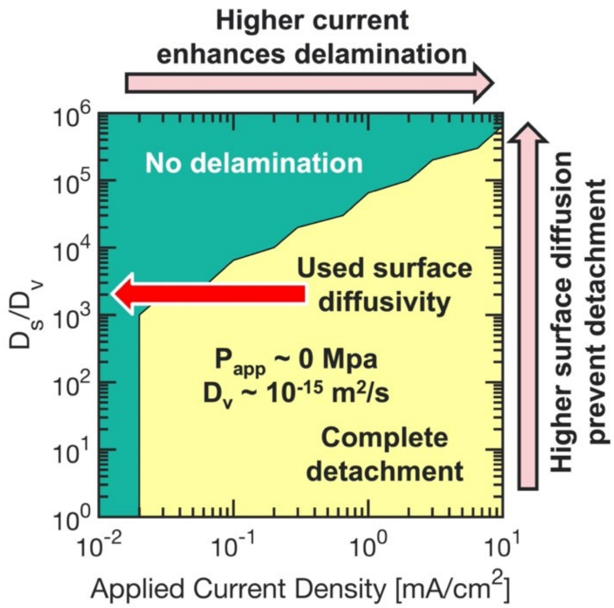

Figure 4. Phase map between surface diffusion coefficient and applied current density indicating the competition between surface diffusivity and current in pore formation and subsequent electrode|electrolyte detachment. Higher surface diffusivity helps to prevent pore formation, whereas larger applied current tends to create pores at the interface. No delamination is observed at lower currents, which is denoted by green/turquoise color. Complete detachment occurs due to pore formation and growth at higher currents, which is shown by yellow. The surface diffusivity used in the present analysis is shown by the red arrow ($D_s/D_v \sim 2000$).

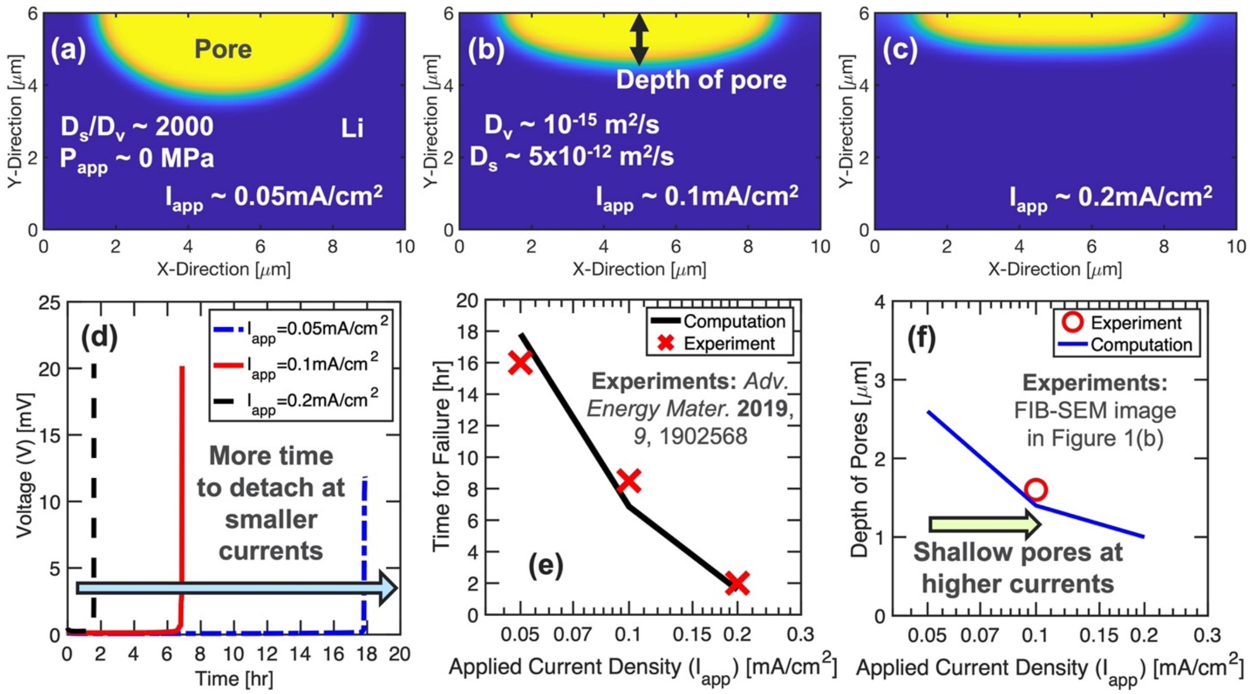

Figure 5. Pore evolution and voltage profile at different current densities and corresponding comparison with experiments. (a) – (c) Profile of pores formed at the lithium|LLZO interface at three different current densities of 0.05 mA/cm^2, 0.1 mA/cm^2, and 0.2 mA/cm^2. The exact magnitude of volumetric (bulk) and surface diffusivities are provided in (b). The surface diffusivity is 2000 times larger than the volumetric diffusivity of lithium, and no external pressure is applied in these simulations. It is evident that the pore depth decreases with increasing applied current density. (d) Voltage vs. time profiles as observed at the three different current densities. It is obvious that more time is required to detach at smaller currents. (e) Comparison of computationally estimated "time to cell failure" at different current densities with experimental results obtained from existing literature. (f) Comparison of computationally predicted and experimentally observed depth of pores at different current densities. The experimental value for depth of pore is extracted from the SEM image shown in Figure 1(b). A decent correlation for the "time to cell failure" and pore depth provides a good validation for the developed phase field based computational model.

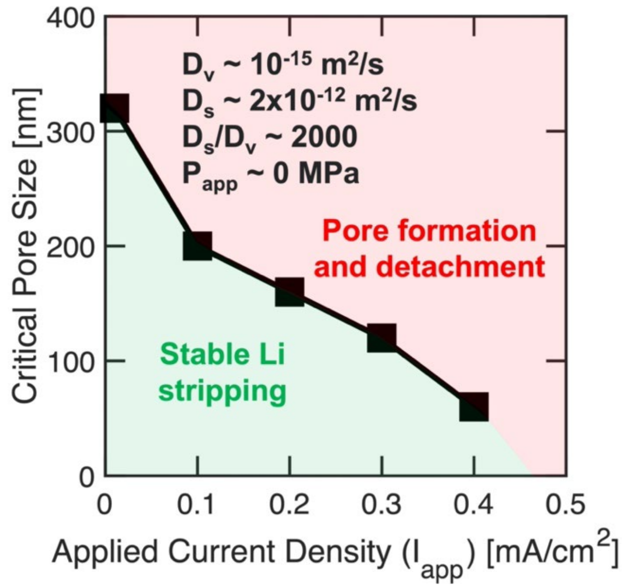

Figure 6. Minimum void size needed to form a spanning pore at the lithium|LLZO interface is characterized as the critical pore size, which depends on the applied current density. With increasing current, the critical pore size decreases. At a particular current density, if the pore is smaller than the critical size, it fails to grow and results in stable stripping of lithium (denoted by the green domain below the black line). Only pores larger than the critical size grow and delaminate the lithium from the solid electrolyte (shown by the red region above the black line). In this particular simulation, the surface diffusivity is maintained 2000 times larger than the bulk diffusivity, and no external pressure was applied.

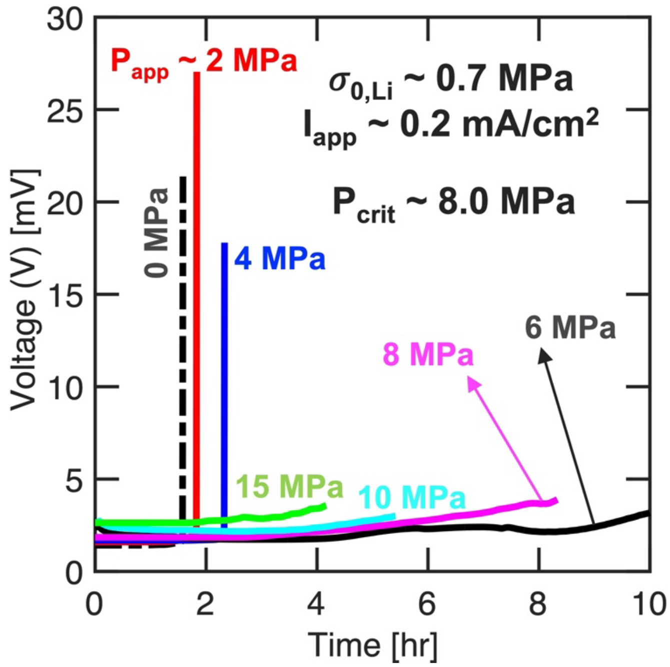

Figure 7. Influence of externally applied pressure on the overall lithium|LLZO detachment and subsequent voltage profile. The applied current density is kept constant at 0.2 mA/cm^2, volumetric (or bulk) and surface diffusivity of lithium is 10^{-15} m^2/s and 2×10^{-12} m^2/s, respectively, which makes the surface diffusivity 2000 times larger than the bulk value, and the yield strength of lithium is assumed to be 0.7 MPa (as reported recently by LePage et al., JES 2019). It is evident that under pressures smaller than 6 MPa quick detachment of the lithium metal electrode occurs from the LLZO electrolyte, and the voltage shoots up quickly. However, at 6 MPa, partial detachment is observed, which continued for a long time. Interestingly, at an externally applied pressure of 8 MPa and higher, complete suppression of the pores occurred. Accordingly, the critical pressure to stabilize lithium stripping at 0.2 mA/cm^2 can be estimated to be around 8 MPa.

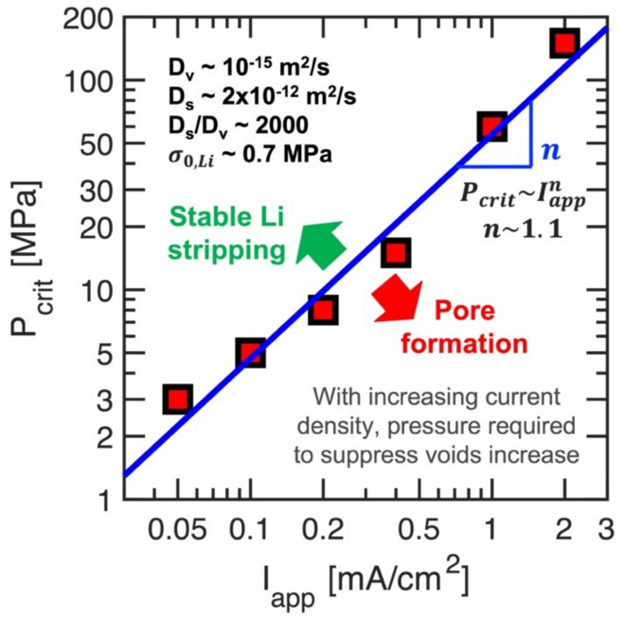

Figure 8. Critical pressure needed to stabilize the lithium stripping process at different current densities. It is evident that there exists a power law relation between critical pressure and applied current density, with a power law exponent of $n = 1.1$. The ratio between surface and bulk diffusion coefficient is maintained constant at 2000 for this analysis, and the lithium yield strength is maintained at 0.7 MPa. Altering either of the two, surface diffusivity or lithium yield strength, can result in a change in the power law relation. At a particular current density, maintaining pressure below the critical value results in pore formation and electrode|electrolyte detachment (shown by the red arrow), whereas application of pressure larger than the critical magnitude leads to stable lithium stripping (depicted by green arrow).

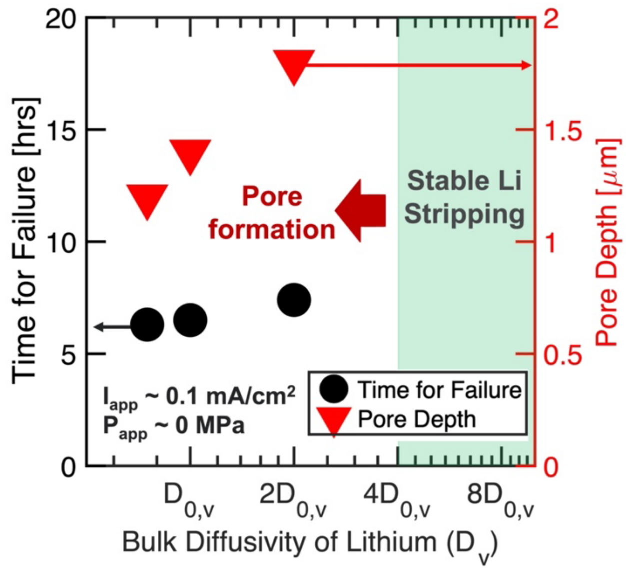

Figure 9. Influence of lithium bulk diffusivity in the pore formation and interfacial detachment is investigated here. Different values of the lithium bulk diffusivities are investigated, starting from $0.5D_{0,v}$ to $8D_{0,v}$, where $D_{0,v}$ is the reference diffusion coefficient for the experimentally observed bulk diffusivity of lithium. Applied current density is maintained at 0.1 mA/cm^2, surface over bulk diffusion coefficient is maintained at 2000, and no external pressure is applied in these simulations. Due to a constant magnitude of D_s/D_v considered in this simulation, the exact magnitude of lithium surface diffusivity also changes along with increasing bulk diffusivity. The time for failure is denoted by the black circles along the left axis, whereas the depth of the pores is indicated by the red triangles along the right axis. Increasing the bulk diffusivity leads to deeper pores that takes longer to delaminate the lithium electrode. Pore formation is observed for bulk diffusivities till $2D_{0,v}$, and no pores form for bulk diffusivities greater than or equal to $4D_{0,v}$. The two domains of stable lithium stripping and pore formation are denoted.

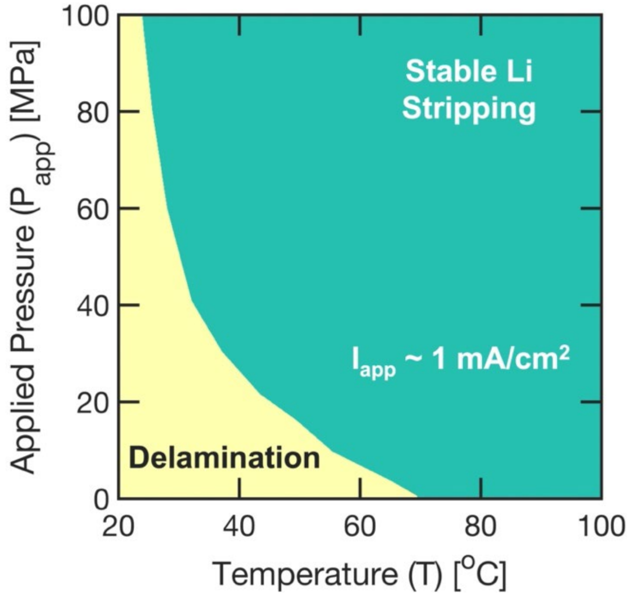

Figure 10. A phase map between externally applied pressure and operating temperature demonstrating the domains where stable stripping of lithium is possible and where delamination should occur. The entire phase map is generated under an applied current density of 1 mA/cm^2. The activation energy for surface and volumetric (or bulk) diffusion of lithium metal is assumed to be similar, which renders a constant magnitude of the D_S/D_v ratio, around 2000. It is evident that increasing both pressure and temperature individually leads to stable stripping of lithium. However, if the temperature and pressure is increased in a combined fashion, stable deposition at 1 mA/cm^2 may be obtained under 40 MPa pressure at 40 °C temperature. Such an improvement in performance at higher temperatures can be attributed to enhanced bulk and surface diffusivities.

TOC Entry

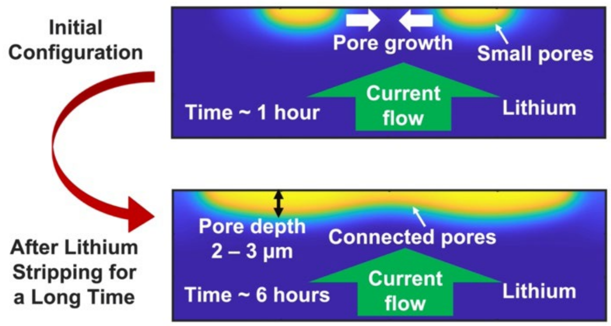

Figure: TOC. Dynamics of pore evolution during stripping of lithium. Initially small sized individual pores form, which grow during stripping, and can coalesce to form larger pore domains.